Metal–Support Interaction

International Edition: DOI: 10.1002/anie.201601823
German Edition: DOI: 10.1002/ange.201601823

Ultrastable Hydroxyapatite/Titanium-Dioxide-Supported Gold Nanocatalyst with Strong Metal–Support Interaction for Carbon Monoxide Oxidation

Hailian Tang, Fei Liu, Jiake Wei, Botao Qiao, Kunfeng Zhao, Yang Su, Changzi Jin, Lin Li, Jingyue (Jimmy) Liu, Junhu Wang,* and Tao Zhang*

Abstract: *Supported Au nanocatalysts have attracted intensive interest because of their unique catalytic properties. Their poor thermal stability, however, presents a major barrier to the practical applications. Here we report an ultrastable Au nanocatalyst by localizing the Au nanoparticles (NPs) in the interfacial regions between the TiO_2 and hydroxyapatite. This unique configuration makes the Au NP surface partially encapsulated due to the strong metal–support interaction and partially exposed and accessible by the reaction molecules. The strong interaction helps stabilizing the Au NPs while the partially exposed Au NP surface provides the active sites for reactions. Such a catalyst not only demonstrated excellent sintering resistance with high activity after calcination at 800 °C but also showed excellent durability that outperforms a commercial three-way catalyst in a simulated practical testing, suggesting great potential for practical applications.*

Gold has long been considered chemically inert, and therefore inactive as a catalytic material. However, since the pioneering works by Haruta et al.[1] and Hutchings.[2] Au nanocatalysts have attracted a great deal of and yet increasing interest in the catalysis field because of their unique catalytic properties.[3] Nevertheless, in contrast to the rapid expansion of fundamental studies, the practical application of supported Au catalysts is severely retarded. The major barrier is the low stability of supported Au catalysts: Au nanoparticles (NPs) tend to sinter and deactivate easily during reaction. This severely inhibited their practical applications, especially at elevated temperatures.[4] For example, supported Au catalysts were suggested to be promising for automotive pollution control[5] in which there is a need to convert CO at low temperatures.[6] The Au catalysts are highly active for CO oxidation even at ambient temperatures which is far below the designated challenging requirement of 150 °C.[7] However, the catalysts used in modern cars have to stand temperatures in excess of 800 °C, which can cause severe sintering of Au NPs.[5a,8] Actually, the activity degradation caused by sintering of noble metals has been one of the biggest issues for the three way catalyst (TWC).[9]

The lower stability of Au catalysts is mainly because of the low Tammann temperature of Au (395 °C).[10] A detailed study, which concluded that the sintering of Au NPs would accelerate upon calcination at temperatures higher than 400 °C, further confirms the sintering issue of Au NPs.[11] So far only a few catalysts have shown good sintering resistance to calcination at temperatures of 500–600 °C[12] while almost no report to demonstrate that Au nanocatalysts could stand calcination temperatures above 600 °C.[13] Therefore, it still remains a formidable challenge to fabricate ultrastable Au nanocatalysts with high activity for practical applications.

Recently, we discovered that Au NPs, upon high-temperature calcination, interact strongly with the hydroxyapatite (HAP) support, resulting in the encapsulation of the Au NPs by a thin layer of HAP-like species (denoted as HAPS which originate from HAP without a known stoichiometry).[14] Such encapsulation of the Au NPs improves their sintering resistance significantly. However, the full encapsulation of the Au NPs reduces their activity due to the coverage of the active sites. Therefore, by controlling the degree of encapsulation of the Au NPs we should be able to fabricate ultrastable supported Au NPs with improved activity. Such utilization of the strong metal–support interaction (SMSI) to stabilize supported Au NPs while maintaining their high activity may provide a novel route for developing practical supported Au catalysts. In this work, we presented an example of manipulating the SMSI between Au and HAP (i.e., the degree of encapsulation) by incorporating TiO_2, a widely used active support for Au nanocatalysts, into the support. By this unique nanoscale architectural design, we found that the supported Au nanocatalysts not only possessed high activity and good sintering resistance after calcination at 800 °C for a variety of

[*] H. Tang, Dr. F. Liu, Dr. B. Qiao, Y. Su, Dr. C. Jin, Dr. L. Li, Prof. J. Wang, Prof. T. Zhang
State Key Laboratory of Catalysis
Dalian Institute of Chemical Physics
Chinese Academy of Sciences
Dalian 116023 (China)
E-mail: bqiao@dicp.ac.cn
wangjh@dicp.ac.cn
H. Tang, Dr. C. Jin, Prof. J. Wang, Prof. T. Zhang
Mössbauer Effect Data Center
Dalian Institute of Chemical Physics
Chinese Academy of Sciences
Dalian 116023 (China)
H. Tang
University of Chinese Academy of Sciences
Beijing 100049 (China)
J. Wei, Prof. J. Liu
Department of Physics, Arizona State University
Tempe, AZ 85287 (USA)
Dr. K. Zhao
National Engineering Research Center for Nanotechnology
Shanghai, 200241 (China)

Supporting information for this article can be found under: http://dx.doi.org/10.1002/anie.201601823.

reactions but also demonstrated excellent durability that outperforms a commercial TWC for CO oxidation under simulated practical conditions. This work significantly lowers the barrier to practical applications of supported Au nanocatalysts, especially for high-temperature catalytic reactions.

Three sets of Au catalysts were prepared. TiO_2 supported Au catalysts with or without calcination at 800 °C were denoted as Au/T-UC and Au/T-800, respectively. Similarly, HAP and TiO_2-HAP supported Au catalysts with or without calcination 800 °C were denoted as Au/H-UC, Au/H-800, Au/TH-UC and Au/TH-800, respectively. The details for the support synthesis and the catalyst preparation were presented in the Supporting Information.

The samples were first examined by transmission electron microscopy (TEM). As shown in Figure S1 (see the Supporting Information), the Au NPs with a mean size of about 3.5 nm are clearly observed in the Au/T-UC sample (Figure S1 a) and all the Au NPs are <2 nm in the Au/H-UC sample (Figure S1 b). For the Au/TH-UC sample, both smaller Au NPs (<2 nm) and some relatively larger Au NPs (ca. 3 nm, as indicated by the arrows in Figure S1 c) are observed which might be ascribed to the Au NPs located on the surfaces of HAP and TiO_2, respectively. After being calcined at 800 °C, the Au NPs sintered severely in the Au/T-800 sample and their mean size dramatically increased to about 32.5 nm (Figure 1 a and Table S1). However, for the Au/H-800 and Au/TH-800 samples the Au NPs only increased to about 8.5 and 8.6 nm, respectively (Figure 1 b,c). These results were further confirmed by X-ray diffraction (XRD) measurements. As shown in Figure S2, no Au diffraction peaks are detected for the catalysts without calcination, indicating that the Au NPs are highly dispersed. After calcination at 800 °C, diffuse diffraction peaks of Au (111) are observed for both the Au/H-800 and Au/TH-800 samples but it is much sharper for the Au/T-800 sample (Figure S2 b), suggesting much larger Au NPs. In addition to the diffraction peaks of Au NPs, diffraction peaks of TiO_2 are also seen. For the Au/T-UC and Au/TH-UC samples TiO_2 exists mainly as anatase (ca. 77 % anatase vs. 23 % rutile, Table S2). After being calcined at 800 °C the anatase phase of TiO_2 in the Au/T-800 sample transformed to the rutile phase completely. However, for the Au/TH-800 sample TiO_2 still existed mainly as anatase (ca. 68 %), suggesting that the phase transformation from anatase to rutile was significantly inhibited. This inhibition must have originated from the interaction between TiO_2 and HAP since the TiO_2 in the Au/TH sample is exactly the same as that in the Au/T sample except the interaction with HAP.

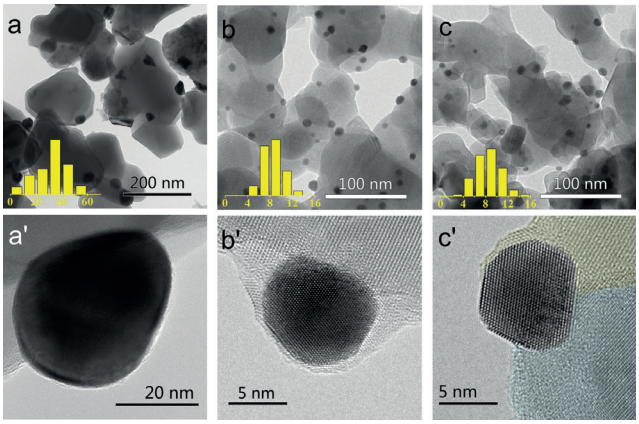

Figure 1. TEM images (top row) and HRTEM images (bottom row) of Au/T-800 (a,a′), Au/H-800 (b,b′) and Au/TH-800 (c,c′) and the corresponding size distributions of Au NPs. The size distributions were obtained by analyzing 200–400 Au NPs from TEM images (The horizontal ordinate is in nanometer and the vertical ordinate represents percentage).

We performed X-ray photoelectron spectroscopy (XPS) measurements to investigate the Ti species in order to understand this unique interaction (Figure S3 and Table S2). As shown in Figure S3, the Ti $2p_{3/2}$ in the Au/T-UC and the Au/T-800 samples consists of one peak at about 458.5 eV, indicating that the Ti ions are in an octahedral environment.[15] However, the broad Ti $2p_{3/2}$ spectra of the Au/TH-UC and Au/TH-800 samples can be fitted, respectively, into two peaks at about 458.4 eV and 459.1 eV with different ratios. The latter can be assigned to Ti ions in a tetrahedral environment and might originate from the interaction of TiO_2 with HAP.[15,16] The higher ratio of the peak at 459.0 eV in the Au/TH-800 suggests that higher temperature calcination resulted in stronger interaction. No evidence demonstrates the formation of the P-Ti bond since the characteristic peak of P 2p in TiP at 128.6 eV is not observed.[17] However, the relatively lower binding energy (BE) of the P 2p (Figure S4 a) may suggest that the Ti ions interact with the P rather than Ca as almost no change is observed in Ca 2p (Figure S4 b). Actually, a previous study on the phosphorus-doped TiO_2[16b] presented a similar conclusion, supporting the above conjecture.

According to our recent discovery,[14] the presence of the smaller Au NPs in the Au/H-800 is a result of the SMSI with the encapsulation of the Au NPs that suppressed their sintering. The presence of these thin encapsulation layers are clearly observable in the high-resolution TEM (HRTEM) images (Figure 1 b′ and Figure S5 a,b). In contrast, the much larger Au NPs in the Au/T-800 were not encapsulated (Figure 1 a′), showing that just TiO_2 cannot stabilize the Au NPs. From this perspective, both smaller Au NPs with a size about 8 nm (similar to those in the Au/H-800) and larger Au NPs (ca. 32.5 nm, similar to those in the Au/T-800) should be observed in the Au/TH-800 sample. However, no large Au NPs are detected in the Au/TH-800 sample (Figure 1 c). More interestingly, it was found that the Au NPs were primarily located at the interfaces between the crystalline particles of the TiO_2 and HAP (Figure S6) in the Au/TH-800 sample. Such unique positioning of the Au NPs has been previously reported.[11] The HRTEM images in Figure 1 c′ and Figure S5 c–f show clearly that the Au NPs are only partially covered by a thin layer. Electron energy loss spectroscopy (EELS) was further employed to examine the composition of the surface species in contact with Au NPs. As shown in Figure S7, the support adjacent to the uncovered Au part is composed of Ti and O while the other side adjacent to the covered Au surface is composed of Ca, Ti, and O, suggesting

that the support is mainly TiO_2 and a mixture of TiO_2 and HAP, respectively.

The above results clearly show that the encapsulation of Au NPs by HAPS layer with SMSI was successfully tuned by introducing TiO_2 in the HAP support. The change of the degree of encapsulation of the Au NPs should change their adsorption behavior since the exposed Au sites are generally regarded as the adsorption sites. In situ diffuse reflectance infrared Fourier transform spectroscopy (DRIFTS) of CO adsorption was performed to evaluate the change of the adsorption sites. As shown in Figure 2a, for the non-calcined

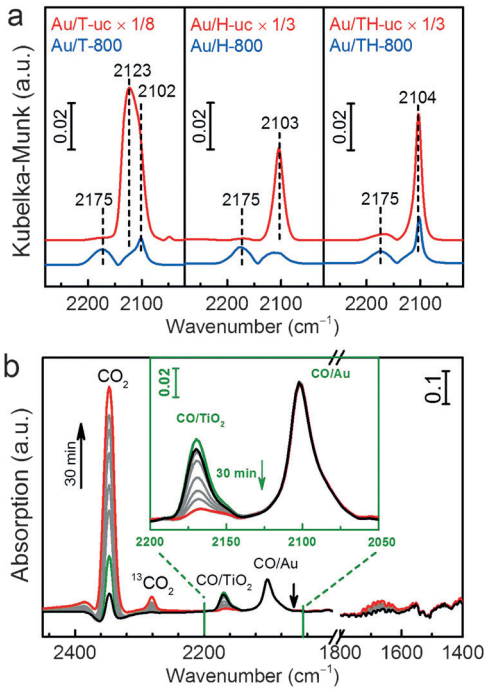

Figure 2. a) In situ DRIFT spectra of CO adsorption on various Au catalysts at room temperature after 10 minutes adsorption; b) The evolution of in situ DRIFT spectra at −130 °C after introducing 15 torr O_2 to the CO preadsorbed Au/TH-800.

samples, there are obvious CO adsorption bands with the strength higher for the Au/T-UC than that for the Au/H-UC and Au/TH-UC. The bands centered at about 2103 cm^{-1} on the Au/H-UC and Au/TH-UC suggest a metallic Au surface. However, the broad and slightly blue-shifted band at 2123 cm^{-1} for the Au/T-UC suggests that the Au surface species are a mixture of metallic Au^0 and positively charged Au^{x+}. After calcination at 800 °C, all CO adsorption bands decreased significantly. For the Au/T-800 only a very weak band centered at 2102 cm^{-1} is observed besides the gas phase CO bands (2175 and 2120 cm^{-1}). The dramatically decreased CO adsorption is a result of the severe sintering of Au NPs on Au/T-800 resulting in the dramatic decrease of the total number of the adsorption sites. The red-shift of the adsorption peak is due to the reduction of the positively charged Au species. For the Au/H-800 only a negligible CO adsorption can be observed, suggesting that the Au NPs were almost completely covered by HAPS.[14] On the other hand, the Au/TH-800 exhibited a much stronger band intensity of CO adsorption, demonstrating a partially covered and relatively small Au NPs. A quantitative analysis of the spectra revealed that almost all the particles existed as half-encapsulated (see method section in the SI for details), consistent with the TEM result that the Au NPs existed primarily at the TiO_2 and HAP interfaces and were partial encapsulated.

The XPS spectra of the Au 4f were further measured to determine the valance state of Au and the possible interaction between Au and the supports. As shown in Figure S8, without calcination Au species on all three supports are a mixture of Au^0 and Au^{x+}, in line with previous reports.[12c,18] The existence of Au^{x+} in the Au/H-UC and Au/TH-UC seems to contradict the result from their DRIFT spectra which suggested that Au existed as metallic Au species. This can be explained by the reduction of Au^{x+} species during CO adsorption.[18] After being calcined at 800 °C, the BE of Au $4f_{7/2}$ in Au/T-800 and Au/H-800 was 83.2 and 83.8 eV, respectively, suggesting the reduction of Au^{x+} to metallic Au. However, the different BE values suggest that the interactions between Au and the supports are different. Thus, the two peaks at 83.8 eV and 83.1 eV in the Au/TH-800 catalyst should be attributed to the Au species in contact with HAP and TiO_2, respectively. This explanation is consistent with the model that the Au NPs were located at the interfaces of TiO_2/HAP and in contact with both the HAP and the TiO_2 nanocrystallites.

Clearly, the incorporation of TiO_2 into HAP has successfully reduced the degree of encapsulation of the Au NPs in the Au/TH-800 catalyst by tuning the SMSI between Au and HAP without affecting the stabilization of the Au NPs. The unique structure that the Au NPs are only partially covered and are in direct contact with the TiO_2 support is not only essential to tuning the encapsulation of Au NPs but also of great importance in improving their catalytic performance for oxidation reactions since HAP is usually regarded as an "inert" support that cannot effectively activate O_2.[19] Recently, Yates et al. discovered a new mechanism of CO oxidation at cryogenic temperature (−150 °C) on Au/TiO_2, that is the CO molecules adsorbed on the TiO_2 sites diffused to the Au–TiO_2 interfaces and reacted with the activated O_2 at the Au–TiO_2 interfaces.[20] This finding not only demonstrated the important role of TiO_2 in CO oxidation, but also provided a new method to examine the interfaces between the metal NPs and the TiO_2 support.[21] To verify whether the TiO_2 species are exposed and are in contact with the Au NPs, we performed a DRIFTS measurement at −130 °C. As shown in Figure 2b, after the introduction of 2 torr CO, three bands centered at 2102, 2170 and 2347 cm^{-1} are clearly observed (the black line in Figure 2b). The former two bands are attributed to the CO adsorbed on Au and TiO_2 sites, respectively.[20,22] The latter one can be assigned to the physisorption of CO_2.[23] After the introduction of 15 torr O_2, the 2170 cm^{-1} band decreased gradually with the increasing of the band at 2347 cm^{-1} and almost no change of the 2102 cm^{-1} band, suggesting that the CO molecules adsorbed on the TiO_2 sites diffused and reacted with O_2 which were activated at the interfaces of Au and TiO_2. In contrast, as a control, no change of the CO adsorption on TiO_2 was

detected for a TH-800 support after the introduction of O_2, (Figure S9), suggesting the importance of forming the Au–TiO_2 interfaces for the CO oxidation reaction.

CO oxidation was firstly employed as a probe reaction due to its great importance in both fundamental study and practical applications for many fields.[24] As shown in Figure 3a and Table S1, for the catalysts without calcination, the

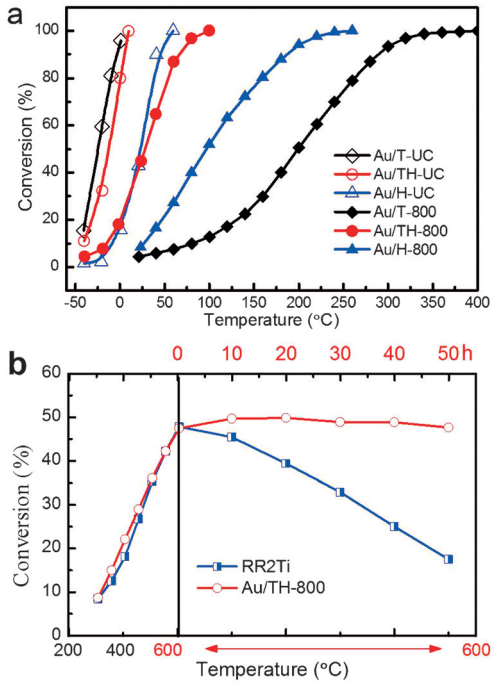

Figure 3. a) CO oxidation curves of Au/X-UC and Au/X-800. Gas flow: 1 v% CO + 1 v% O_2 and balanced with He, 33.3 mL min^{-1}, 100 mg catalyst, space velocity (SV) = 20000 mL g_{cat}^{-1} h^{-1}; b) The catalytic performance for RWGS reaction of Au/TH-800 and RR2Ti. The temperature increased from 300 to 600 °C with a rate of 2.5 °C min^{-1} then maintained at 600 °C for 50 h. Gas flow: 20 mL min^{-1}, 100 mg catalyst, 10 v% CO_2 + 10 v% H_2 and balanced with He. SV = 12000 mL g_{cat}^{-1} h^{-1}.

Au/T-UC exhibited the highest activity with a T50 (the temperature at which 50% CO conversion is achieved) of −25 °C and the Au/H-UC exhibited the lowest activity with a T50 of 24 °C. The Au/TH-UC shows a similar activity to that of the Au/T-UC with a T50 of −12 °C, suggesting that the activity may be mainly contributed by the combination of Au–TiO_2 rather than Au–HAP. After calcination at 800 °C, the activity of Au/H-800 and Au/T-800 decreased significantly with a T50 of about 100 and 200 °C, respectively. According to TEM and DRIFT characterizations, the decreased activity of the Au/T-800 is due to the significant sintering of the Au NPs while for the Au/H-800 the encapsulation of the Au NPs by HAPS significantly reduced the number of the Au active sites. Comparatively, the Au/TH-800 exhibited a quite impressive activity with a much lower T50 of 27 °C, suggesting the significant effect of tuning the degree of encapsulation of the Au NPs.

In order to compare the intrinsic activity of the above catalysts, we measured their specific rates and calculated the corresponding TOFs at 25 °C (Table S1). For the catalysts without calcination, both the reaction rates and TOFs are in the order of Au/T-UC > Au/TH-UC > Au/H-UC, in line with the above results. After calcination at 800 °C, different extents of decrease in activity are observed: for the Au/TH series, the reaction rate decreased from 1.04 to 0.16 mol_{CO} g_{Au}^{-1} h^{-1}, about seven times less active, much smaller than the about 14 times (0.31 to 0.023 mol_{CO} g_{Au}^{-1} h^{-1}) of Au/H series and the about 490 times (2.93 to 0.006 mol_{CO} g_{Au}^{-1} h^{-1}) of Au/T series. The specific rates and TOFs of these catalysts before and after calcination are presented in Figure S10 in a histogram form. It gives a visual comparison and reflects the sintering resistance of these catalysts clearly. To further evaluate the activity of the Au/TH-800 catalyst, the specific rates and/or TOFs of some representative catalysts reported previously were also listed in Table S1 for comparison. We can see that our Au/TH-800 catalyst is as active as the standard Au catalyst of 4.4 wt % Au/Fe_2O_3 (provided by World Gold Council, WGC) which represents one type of the most active Au catalysts.[25] It is also comparable (TOF) to, or slightly less active (specific rate) than, the Au/Al_2O_3-700 and Au/TiO_2-SiO_2-800 which are, to our knowledge, the Au-based catalysts with best sintering resistance.[13] In addition, with a lower Au loading (1.0 wt %) the Au/TH-800 has smaller Au NPs (mean size of ca. 4.9 nm, Figure S11) and thus presents an enhanced specific rate and TOF value, suggesting that the catalyst formula could be further optimized. It is worth noting that the activity of our 1.0 wt % Au/TH-800 is only 3–4 times lower than that of the two standard Au/TiO_2 catalysts of RR2Ti (1 wt % Au, supplied by Haruta Gold Inc.) and Au/TiO_2-WGC (provided by WGC). For comparison, the Au/TiO_2-WGC catalyst after calcination at 800 °C is inactive at temperatures below 200 °C (Figure S12) and their TOF is undetectable at ambient temperatures.

The sintering of Au NPs is regarded as the main reason for the deactivation of supported Au catalyst for CO oxidation, especially at high temperatures.[26] Since our Au/TH-800 had good sintering resistance, we can reasonably expect a good reaction stability of this catalyst. We verified this by testing CO oxidation at 400 °C with a relatively low conversion to avoid the activity saturation. As shown in Figure S13a, the conversion kept unchanged during a 100-hour test, showing excellent stability. To our knowledge, this is the best result so far for supported Au catalysts, even better than the stability of the recently reported single-atom Au_1/FeO_x catalyst.[26] The stability was further tested at 30 °C where the accumulation of carbonates is generally responsible for the deactivation.[18] As shown in Figure S13b, the conversion is nearly constant in the 60 hour-test, demonstrating the good CO_2 resistance property of our catalyst. We also tested the recycle performance of our catalyst since in practical applications the catalyst may need to go through cold-hot cycling frequently. As shown in Figure S14, in six cycles running up to 800 °C the catalyst performance did not degrade.

Water is usually thought to accelerate the sintering of metal particles.[26,27] To evaluate the stability of our Au/TH-800 in the presence of water, reverse water gas shift (RWGS) reaction was further investigated. It is a typical high-temperature reaction and had attracted attention in recent years due

to its importance in CO_2 activation and utilization. As shown in Figure 3b, our Au/TH-800 showed a similar activity to the RR2Ti with the CO_2 conversion increasing gradually to about 50% at 600°C, corresponding to a generation of 5 v% H_2O in the reaction system. In a further 50-hour test at 600°C no obvious decrease of CO_2 conversion is observed, suggesting the strong anti-sintering property of the Au/TH-800. The analysis of the used catalyst, as expected, showed that the mean size of the Au NPs in the Au/TH-800 was only slightly increased (from 8.6 to 9.3 nm, Figure S15) while the ratio of anatase to rutile remained almost unchanged (not shown), demonstrating the structural stability of the Au/TH-800. In contrast, the RR2Ti catalyst, employed as a reference catalyst, deactivated gradually during the 50-hour test.

The above results unambiguously show that our Au/TH-800 catalyst is not only highly active but also extremely stable at elevated temperatures even in the presence of water. Such catalyst characteristics imply a great potential for practical applications. We further exemplified this by using CO emission control in a simulated mixture of 1.6 v% CO, 1 v% O_2, 0.01 v% propene, 0.0087 v% toluene, 10 v% water and balanced with He[13b] and used a commercial TWC (JM888, Johnson Matthey) as a reference. As shown in Figure 4, the CO conversion for the TWC of JM888 decreased

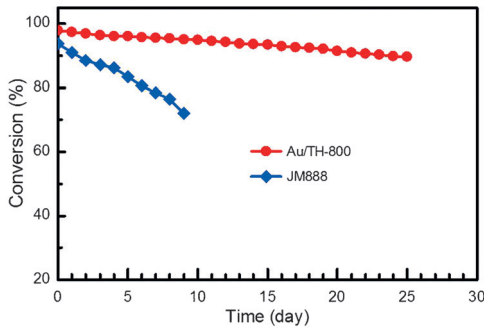

Figure 4. The CO conversion curves as a function of reaction time on the Au/TH-800 (10 mg) and TWC of JM888 (5.4 mg) at 400°C with SV of 200 $L g_{cat}^{-1} h^{-1}$ and 1100 $L g_{cat}^{-1} h^{-1}$, respectively. Reaction gas composition: 1.6 v% CO, 1 v% O_2, 0.01 v% propene, 0.0087 v% toluene, 10 v% water and balanced with He.

from 94% to 72% within a test of 9 days. Our Au/TH-800, however, exhibited a much better durability with a gradual decrease of CO conversion from 98% to 90% in a test of 25 days, suggesting its excellent stability under practical application conditions.

In summary, we have developed an ultrastable and highly active Au nanocatalyst by tuning the SMSI between Au and the support. Au NPs were stabilized at the interfaces of the TiO_2 and HAP nanocrystallites. The strong interaction between Au and HAP and the partially covered Au NPs by HAPS account for the thermal stability of the Au NPs while the partially exposed Au NPs, which are in direct contact with TiO_2, provide the enhanced activity. As a result, the designed catalyst possesses both high catalytic activity and good sintering-resistance and thus excellent reaction stability. In addition, the application of this type of catalysts in the reactions involving organic compounds might be expected since HAP has special adsorptivity for a variety of organic compounds.[28] Of more importance, this work may provide a new strategy to develop ultrastable Au nanocatalysts with high activity by designing and tuning the SMSI.

Experimental Section

The Au catalysts were prepared by a deposition-precipitation method.[12c] Typically, 1.0 g support was added into $HAuCl_4$ solution (1.25 $mg_{Au} mL^{-1}$) of which the pH was pre-adjusted to about 9 by addition of NaOH solution (0.1 $mol L^{-1}$). The solution was kept at pH about 9 for 1.0 h, followed by a heating at 65°C for another 1 h. Then the precipitates were filtered, washed with deionized water and dried at 60°C overnight. Finally, the product was divided into two parts, one part without any further treatment was denoted as Au/X-UC (where X is H, T and HT, representing HAP, TiO_2, and HAP-TiO_2, respectively), and the other part was denoted as Au/X-800 after further calcination at 800°C for 3.0 h.

The details of the catalyst preparation, activity tests, and the characterizations are given in the Supporting Information.

Acknowledgements

This work was supported by National Natural Science Foundation of China (grant numbers 21476232, 21303184). J.W. and J.L. acknowledge the support by the College of Liberal Arts and Sciences of Arizona State University and the National Science Foundation under grant number CHE-1465057. The authors acknowledge the use of facilities in the John M. Cowley Center for High Resolution Electron Microscopy at Arizona State University.

Keywords: gold · heterogeneous catalysis · metal–support interactions · nanoparticles · surface chemistry

How to cite: *Angew. Chem. Int. Ed.* **2016**, *55*, 10606–10611
Angew. Chem. **2016**, *128*, 10764–10769

[1] a) M. Haruta, T. Kobayashi, H. Sano, N. Yamada, *Chem. Lett.* **1987**, 405–408; b) M. Haruta, N. Yamada, T. Kobayashi, S. Iijima, *J. Catal.* **1989**, *115*, 301–309.
[2] G. J. Hutchings, *J. Catal.* **1985**, *96*, 292–295.
[3] M. Turner, V. B. Golovko, O. P. H. Vaughan, P. Abdulkin, A. Berenguer-Murcia, M. S. Tikhov, B. F. G. Johnson, R. M. Lambert, *Nature* **2008**, *454*, 981–983.
[4] C. W. Corti, R. J. Holliday, D. T. Thompson, *Top. Catal.* **2007**, *44*, 331–343.
[5] a) G. Pattrick, E. van der Lingen, C. W. Corti, R. J. Holliday, D. T. Thompson, *Top. Catal.* **2004**, *30*, 273–279; b) C. W. Corti, R. J. Holliday, D. T. Thompson, *Appl. Catal. A* **2005**, *291*, 253–261.
[6] E. J. Peterson, A. T. DeLaRiva, S. Lin, R. S. Johnson, H. Guo, J. T. Miller, J. Hun Kwak, C. H. F. Peden, B. Kiefer, L. F. Allard, F. H. Ribeiro, A. K. Datye, *Nat. Commun.* **2014**, *5*, 4885.
[7] Future Automotive Aftertreatment Solutions: The 150°C Challenge. USDRIVE Workshop **2012**.
[8] Y. Nagai, K. Dohmae, Y. Ikeda, N. Takagi, T. Tanabe, N. Hara, G. Guilera, S. Pascarelli, M. A. Newton, O. Kuno, H. Jiang, H. Shinjoh, S. i. Matsumoto, *Angew. Chem. Int. Ed.* **2008**, *47*, 9303–9306; *Angew. Chem.* **2008**, *120*, 9443–9446.
[9] H. Shinjoh, *Catal. Surv. Asia* **2009**, *13*, 184–190.
[10] S. E. Golunski, *Platinum Met. Rev.* **2007**, *51*, 162–162.

[11] T. Akita, P. Lu, S. Ichikawa, K. Tanaka, M. Haruta, *Surf. Interface Anal.* **2001**, *31*, 73 – 78.
[12] a) W. Yan, S. M. Mahurin, Z. Pan, S. H. Overbury, S. Dai, *J. Am. Chem. Soc.* **2005**, *127*, 10480 – 10481; b) W. Yan, S. Brown, Z. Pan, S. M. Mahurin, S. H. Overbury, S. Dai, *Angew. Chem. Int. Ed.* **2006**, *45*, 3614 – 3618; *Angew. Chem.* **2006**, *118*, 3696 – 3700; c) K. Zhao, B. Qiao, J. Wang, Y. Zhang, T. Zhang, *Chem. Commun.* **2011**, *47*, 1779 – 1781; d) J. Liu, B. Qiao, Y. Song, Y. Huang, J. J. Liu, *Chem. Commun.* **2015**, *51*, 15332 – 15335.
[13] a) J. Wang, A. H. Lu, M. Li, W. Zhang, Y. S. Chen, D. X. Tian, W. C. Li, *ACS Nano* **2013**, *7*, 4902 – 4910; b) B. Puértolas, Á. Mayoral, R. Arenal, B. Solsona, A. Moragues, S. Murcia-Mascaros, P. Amorós, A. B. Hungría, S. H. Taylor, T. García, *ACS Catal.* **2015**, *5*, 1078 – 1086.
[14] H. Tang, J. Wei, F. Liu, B. Qiao, X. Pan, L. Li, J. Liu, J. Wang, T. Zhang, *J. Am. Chem. Soc.* **2016**, *138*, 56 – 59.
[15] A. A. S. Alfaya, Y. Gushikem, *Chem. Mater.* **1998**, *10*, 909 – 913.
[16] a) J. C. Yu, L. Zhang, Z. Zheng, J. Zhao, *Chem. Mater.* **2003**, *15*, 2280 – 2286; b) S. Guo, S. Han, H. Mao, C. Zeng, Y. Sun, B. Chi, J. Pu, J. Li, *Mater. Res. Bull.* **2013**, *48*, 3032 – 3036.
[17] S. Baunack, S. Oswald, D. Scharnweber, *Surf. Interface Anal.* **1998**, *26*, 471 – 479.
[18] K. Zhao, H. Tang, B. Qiao, L. Li, J. Wang, *ACS Catal.* **2015**, *5*, 3528 – 3539.
[19] a) J. Huang, L.-C. Wang, Y.-M. Liu, Y. Cao, H.-Y. He, K.-N. Fan, *Appl. Catal. B* **2011**, *101*, 560 – 569; b) K. Zhao, B. Qiao, Y. Zhang, J. Wang, *Chin. J. Catal.* **2013**, *34*, 1386 – 1394.
[20] I. X. Green, W. Tang, M. Neurock, J. T. Yates, Jr., *Science* **2011**, *333*, 736 – 739.
[21] H. Guan, J. Lin, B. Qiao, X. Yang, L. Li, S. Miao, J. Liu, A. Wang, X. Wang, T. Zhang, *Angew. Chem. Int. Ed.* **2016**, *55*, 2820 – 2824; *Angew. Chem.* **2016**, *128*, 2870 – 2874.
[22] I. Lee, J. B. Joo, Y. Yin, F. Zaera, *Angew. Chem. Int. Ed.* **2011**, *50*, 10208 – 10211; *Angew. Chem.* **2011**, *123*, 10390 – 10393.
[23] F. Boccuzzi, A. Chiorino, *J. Phys. Chem. B* **2000**, *104*, 5414 – 5416.
[24] H. J. Freund, G. Meijer, M. Scheffler, R. Schlogl, M. Wolf, *Angew. Chem. Int. Ed.* **2011**, *50*, 10064 – 10094; *Angew. Chem.* **2011**, *123*, 10242 – 10275.
[25] B. Qiao, A. Wang, X. Yang, L. F. Allard, Z. Jiang, Y. Cui, J. Liu, J. Li, T. Zhang, *Nat. Chem.* **2011**, *3*, 634 – 641.
[26] B. Qiao, J.-X. Liang, A. Wang, C.-Q. Xu, J. Li, T. Zhang, J. J. Liu, *Nano Res.* **2015**, *8*, 2913 – 2924.
[27] C. H. Bartholomew, *Appl. Catal. A* **2001**, *212*, 17 – 60.
[28] a) R. P. Scott, A. M. Jackson, A. D. Wilson, *Biomaterials* **1990**, *11*, 341 – 344; b) J. Ellis, A. M. Jackson, B. P. Scott, A. D. Wilson, *Biomaterials* **1990**, *11*, 379 – 384.

Received: February 22, 2016
Revised: May 16, 2016
Published online: July 27, 2016

